Journal of Power Sources 230 (2013) 96–100

Contents lists available at SciVerse ScienceDirect

Journal of Power Sources

journal homepage: www.elsevier.com/locate/jpowsour

Short communication

One-dimensional manganese oxide nanostructures as radical scavenger to improve membrane electrolyte assembly durability of proton exchange membrane fuel cells

M. Lei [a,b], T.Z. Yang [c,*], W.J. Wang [c], K. Huang [b], Y.C. Zhang [b], R. Zhang [a,b], R.Z. Jiao [a,b], X.L. Fu [a,b], H.J. Yang [b], Y.G. Wang [b], W.H. Tang [a,b]

[a] State Key Laboratory of Information Photonics and Optical Communications, Beijing University of Posts and Telecommunications, Beijing 100876, China
[b] School of Science, Beijing University of Posts and Telecommunications, Beijing 100876, China
[c] Beijing National Laboratory for Condensed Matter Physics, Institute of Physics, Chinese Academy of Sciences, Beijing 100190, China

HIGHLIGHTS

- 1D MnO_2 nanotubes and nanowires are synthesized by facile hydrothermal routes.
- 1D MnO_2 is effective in minimizing the radical degradation in PEM fuel cells.
- Water retention of the hydrophilic MnO_2 reduces the humidity sensitivity of fuel cells.

ARTICLE INFO

Article history:
Received 4 October 2012
Received in revised form
16 November 2012
Accepted 3 December 2012
Available online 12 December 2012

Keywords:
Manganese oxide
Nanowires
Nanotubes
Proton exchange membrane fuel cell
Radical degradation

ABSTRACT

One-dimensional manganese oxide (MnO_2) scavengers are proposed to minimize the radical degradation of membrane electrode assembly (MEA) in fuel cells. The synthesized MnO_2 nanotubes and MnO_2 nanowires are *ca.* 5–8 nm in diameter and more than 100 nm in length, respectively. Water retention of the hydrophilic MnO_2 reduces the humidity sensitivity of the fuel cells. At 75 RH% humidify levels of inlet gas at 60 °C, single cells assembled by catalyst layer with MnO_2 nanotubes and nanowires as the cathodes have peak power densities of 599.3 and 536.8 mW cm^{-2}, respectively. Radical scavenger MnO_2 in the cathode catalyst is effective in minimizing the radical degradation in proton exchange membrane (PEM) fuel cells. After the OCV degradation, the hydrogen crossover of cell assembled by catalyst layer with MnO_2 nanowires or MnO_2 nanotubes in anode and traditional catalyst layer in cathode are about 5.3 and 4.9 mA cm^{-2}, respectively. As a comparison, single cell with conventional catalyst layer in both anode and cathode, the hydrogen crossover through the MEA is increased to 14.7 mA cm^{-2}.

1. Introduction

The durability of proton exchange membrane (PEM) fuel cells, especially when the fuel cell is operated in transportation with extreme or cyclic changes in load, is one of the biggest challenges and barriers for commercializing this promising technology [1,2]. Currently, considerable researches have concentrated on reducing the wide gap that exists between the ideal and the state-of-the-art lifetimes of PEM fuel cells [3]. Chemical degradation of the electrolyte in the catalyst layer or proton exchange membrane is reported to be a major cause of PEFC lifetime limitations. It is generally accepted that chemical degradation of the electrolyte occurs via a two-step process [4–6], including the formation of reactive oxygen species such as the hydroxyl radicals, $OH^{\bullet}$, and reaction of reactive oxygen species with the electrolyte.

In the membrane electrode assembly (MEA) of the PEM fuel cells, the commonly employed carbon supports and Pt catalysts inevitably suffer oxidation during long-term operations in oxygen-rich, high operating-potentials and low pH environments [7–12]. Ionic pathway degradation in the catalyst layer also can be observed due to the chemical degradation of proton conductive electrolyte with radicals [11]. The integrity of the PEM is another crucial factor affecting the lifetime of fuel cells because it functions as both an electrolyte and a separator of the reactant gases. The former decreases the performance, while the latter aggravates the gas crossover through the electrolyte membrane and destroys the

* Corresponding author. Tel./fax: +86 10 82649032.
E-mail address: tzyang@iphy.ac.cn (T.Z. Yang).

0378-7753/$ – see front matter © 2012 Elsevier B.V. All rights reserved.
http://dx.doi.org/10.1016/j.jpowsour.2012.12.011

cell [13,14]. With the hydroxyl radicals, proton conductive electrolyte, such as perfluorinated sulfonic acid ionomers (PFSA), can be unzipped because some unstable terminal–COOH end groups are oxidized to carbon dioxide, reforming the linked CF_2 units to another terminal carboxyl group [15–17].

Hydrogen peroxide and its decomposition intermediate product hydroxyl radicals, $OH^{\bullet}$ that are generated at the fuel cell environment are considered as one of the important factors which leads to the proton conductive electrolyte degradation. Radicals can originate from electrochemical and chemical reactions on fuel cell cathode with the presence of transition metal cations which can split hydrogen peroxide produced from a two-step electron oxygen reduction [18,19], or direct reaction of H_2/O_2 on the surface of the Pt catalyst because of oxygen crossover from the cathode at low currents and hydrogen crossover from the anode at high currents [20–23]. Depending on the catalyst and its surface modification, oxygen reduction reaction (ORR) may go via a four-electron route yielding water, or through a two-electron pathway producing hydrogen peroxide. The yield of H_2O_2 on a typical fuel cell catalyst such as Pt/C can reach 15% [24].

Several strategies are introduced to reduce the effect of reactive oxygen species in a fuel cell. The first is the improvement of the chemical durability of the proton conductive electrolyte by minimizing the unstable terminal–COOH end groups of the perfluorinated sulfonic acid electrolyte. It is proposed that hydrothermal decarboxylation of defect groups with the assistance of counter ions and ethylene glycol can improve the chemical durability of the perfluorinated sulfonic acid by several times of magnitude [6,17]. However, the residual defect groups still constitute a durability hazard for the proton conductive electrolyte. Another approach is to develop peroxide decomposition catalysts in the electrodes [25] or proton exchange membrane [26,27]. It is demonstrated that the Pt/C/MnO_2 hybrid catalysts produced 50% less hydrogen peroxide than the baseline Pt/C electrocatalyst. At 90 °C and 50% RH at open circuit with pure hydrogen as fuel and air as the oxidant, the concentration of F- in the anode condensate over 24 h was found to be reduced by a factor of 3–4 when Pt/C/MnO_2 replaced Pt/C as the catalyst [28].

In this work, we choose MnO_2 as a regenerative free radical scavenger for PEMs owing to its unique acid-based and redox properties. MnO_2 has been demonstrated to be excellent free radical scavengers [29–32]. Additionally, they can be regenerative in nature, especially in acidic media. We here focus on incorporating one-dimensional (1D) MnO_2 scavengers within the catalyst layer to capture reactive oxygen radicals, which further improves membrane electrolyte assembly durability of PEM fuel cells. The preparation procedure and properties of the catalyst layers were studied in detail. The results show that the 1D MnO_2 scavengers possess excellent anti-oxidation abilities. The membrane electrolyte assembly with 1D MnO_2 scavengers evidently lowers the rate of OCV degradation of the fuel cell under accelerated tests.

2. Experimental section

2.1. Preparation of the MnO_2 nanotubes, nanowires and the catalyst layer

The MnO_2 nanotubes were synthesized by a facile hydrothermal method. 2.604 g of $MnSO_4 \cdot 4H_2O$ was dissolved in 400 mL of Nafion solution (5 wt.% in water, Du pont) with vigorous stirring. When the solution was clarified, 23.4 mL of aqueous solution containing 23.4 mmol of $NaClO_3$ was added into the above solution under continuous stirring. The mixture was then transferred into a Teflon-lined stainless steel autoclave. The autoclave was sealed and maintained at 160 °C for 10 h. After the autoclave was cooled to room temperature naturally, black precipitates can be obtained.

The MnO_2 nanowires were synthesized as follows: 1.58 g $KMnO_4$ and 4 mL of formaldehyde were dissolved in 348 mL Nafion solution (5 wt.% in water) and transferred into a Teflon-lined stainless steel autoclave. The synthesis was carried out under hydrothermal conditions at 120 °C for 10 h. The autoclave was cooled to room temperature naturally when the reaction time was finished. The final products were further annealed at 300 °C for 1 h.

Conventional catalyst slurry and the MEA were prepared by following procedures: For catalyst layer with MnO_2, catalyst slurry was prepared before the MEA and catalyst-coated membrane (CCM) fabrication. During the preparation, 1 g Pt/C catalysts (60 wt.% Pt/C, Johnson Matthey) were mixed with 10 mL de-ionized water under vigorous stirring. Then 3.16 g Nafion/MnO_2 nanotubes (or MnO_2 nanowires) were added to the mixture, followed by ultrasonic treatment for 30 min and a high-speed homogenizer (20,000 rpm) for 1 h to form catalyst slurry. After that, the catalyst slurry was applied to PTFE thin film by spraying. After dried at 60 °C for 10 min and followed with at 90 °C in N_2 atmosphere for 3 min, the catalyst layer was then transferred onto the Nafion 211 membrane (Du pont) at 125 °C and 10 MPa by the decal method to form the CCM. The GDL was placed on the anode and cathode side of the CCM to form the MEA. The Pt loading of the anode and cathode catalyst layer was 0.25 mg cm^{-2}.

2.2. Characterizations of the MnO_2 nanotubes, nanowires and the catalyst layer

Transmission electron microscopy (TEM) characterizations of MnO_2 nanotubes and nanowires were carried out on a JEOL 6300 at an accelerating voltage of 120 kV. The performance and durability of MEAs were measured in a single PEM fuel cell on G50 Fuel Cell Test Station (GreenLight) at 60–95 °C without back pressure. In the test, H_2 and air were used as the fuel and the oxidant, respectively. The MEA was mounted in a single cell test fixture with a serpentine flow field and a fuel cell clamp (with an active area of 3×3 cm^2). The H_2 and air flow rates were 300 and 2000 sccm, respectively. The humidity of the H_2 and air was kept at the same level and the cell performance was measured as a function of relative humidity (RH). Prior to measurement, cells were activated by polarization at a constant current until stable performance was reached.

The durability of the MEAs in a single PEM fuel cell was investigated at an open circuit voltage (OCV) on fuel cell test station. The cells were operated under 75 RH% humidify levels of inlet hydrogen and air at 60 °C without back pressure. During the long-term durability tests, the OCV values of the cell were automatically recorded by the G50 Fuel Cell Test Station.

The electrochemical active surface area or activity of the cell estimated from cyclic voltammograms was measured with scan rate of 20 mV s^{-1} at ambient temperatures. Prior to the cyclic voltammograms tests, cell was activated by operating at 1000 mA cm^{-2} with 100 RH% H_2/air for 30 min. Then, dry hydrogen at a flow rate of 10 sccm was fed to the anode (which served as the counter and reference electrodes) and argon to the cathode at 100 sccm, which served as working electrode. The potential was scanned between 0.05 V and 1.2 V versus the cathode (working electrode). Relative electrochemical active surface areas were obtained by comparing the area of hydrogen oxidation peaks from the cyclic voltammograms.

The gas permeability or crossover through membranes was assessed by measuring diffusion-limited hydrogen oxidation current densities of the crossover H_2 using Autolab PG30/FRA. H_2 gas (300 sccm) was fed to the anode side of the cell while N_2 was fed to the cathode. By applying a dynamic potential from 0 to 0.7 V

vs. the anode (i.e., dynamic hydrogen electrode, DHE) at 0.5 mV s^{-1}, the limiting H_2 oxidation current density was measured. The anode side, where hydrogen evolution takes place, served as the counter electrode and the DHE reference electrode.

3. Results and discussion

The morphology and dimension of the as-prepared MnO_2 nanotubes were examined by TEM (Fig. 1a and b). The TEM image (Fig. 1a) clearly reveals the tubular MnO_2. The nanotubes with high quantity are usually 5–8 nm in diameter and more than 100 nm in length. Fig. 1b gives a magnified view of a single tubular crystal, revealing the hollow interior nature of these tubular structures. The diameter of the tubular crystal is *ca.* 5 nm and the thickness of the tube walls is estimated to be 1–2 nm. Fig. 1c and d present TEM images of the MnO_2 nanowires, revealing that the MnO_2 consists of nanowires with diameters ranging from 4 to 6 nm and lengths up to several hundreds of nanometres.

Fig. 2 presents cyclic voltammograms of the conventional catalyst layer, catalyst layer with MnO_2 nanotubes and nanowires. In the left section of the curves, hydrogen on the catalyst surface is desorbed until the catalyst is free of hydrogen at *ca.* 0.35 V. Subsequently, the current observed from 0.35 to 0.7 V is not utilized for electrochemical reaction, but utilized for charging the double layer between the electrode and the electrolyte. The formation of a surface oxide/hydroxide appears above *ca.* 0.75 V. The corresponding electrochemical active surface areas of the catalyst layers were calculated from the H_2 desorption peak of the voltammogram. The corresponding results are 180.2, 178.3 and 177.8 cm^2 cm^{-2} for conventional catalyst layer, catalyst layer with MnO_2 nanotubes and catalyst layer with MnO_2 nanowires, respectively. The electrochemical active surface areas of catalyst layer with MnO_2 are a little smaller than that of conventional catalyst layer, indicating that the small content of MnO_2 in catalyst layer does not seriously affect the available catalyst area in the whole catalyst layer.

At fully humidified condition, the performance of catalyst layer with MnO_2 is no better than that of conventional catalyst layer. Advantage of catalyst layers with MnO_2 in performance arises when the humidity of inlet gas lower than 100 RH%. Fig. 3 shows the performance of single cells assembled with various catalyst layers under 75 RH% humidify levels of inlet gas at 60 °C. A single cell assembled by conventional catalyst layer in both at cathode and anode has peak power density of 430.4 mW cm^{-2}. Single cells

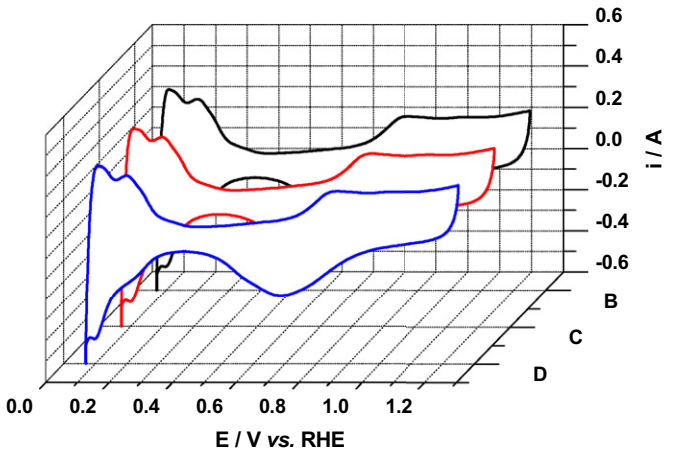

Fig. 2. Cyclic voltammograms of the conventional catalyst layer (line *B*), catalyst layer with MnO_2 nanotubes (line *C*) and catalyst layer with MnO_2 nanowire (line *D*).

assembled by catalyst layer with MnO_2 nanotubes or MnO_2 nanowires in the cathodes and conventional catalyst layer as the anodes have better performances. The peak power densities achieve 551.2 and 536.8 mW cm^{-2}, respectively. These results demonstrate the water retention of the hydrophilic MnO_2 and indicate that the catalyst layer with MnO_2 is much less sensitive towards humidity change of the reactant gases. The peak power densities of cells with MnO_2 nanotubes or MnO_2 nanowires in the anodes and conventional catalyst layer as the cathode have peak power densities of 599.3, 583.2 mW cm^{-2}, slightly lower than the cells with MnO_2 in cathode because the hydrophilic MnO_2 improves the water retention in anode electrodes, thus reduces the proton transportation resistance from the anode to cathode.

Open circuit voltage (OCV) operation has also been recognized as an effective stressor for accelerated testing and the accelerated effects of OCV operation on the degradation of PEM fuel cell components, including the PEM and catalyst layers, have been investigated. The increased gas crossover due to zero reactant consumption under OCV conditions was believed to be the major reason for the electrolyte chemical degradation [33,34]. Fig. 4 shows the open circuit voltage (OCV) degradation of fuel cell with variable catalyst layer. The OCV of the fuel cell assembled with conventional catalyst layer in both at cathode and anode decreased

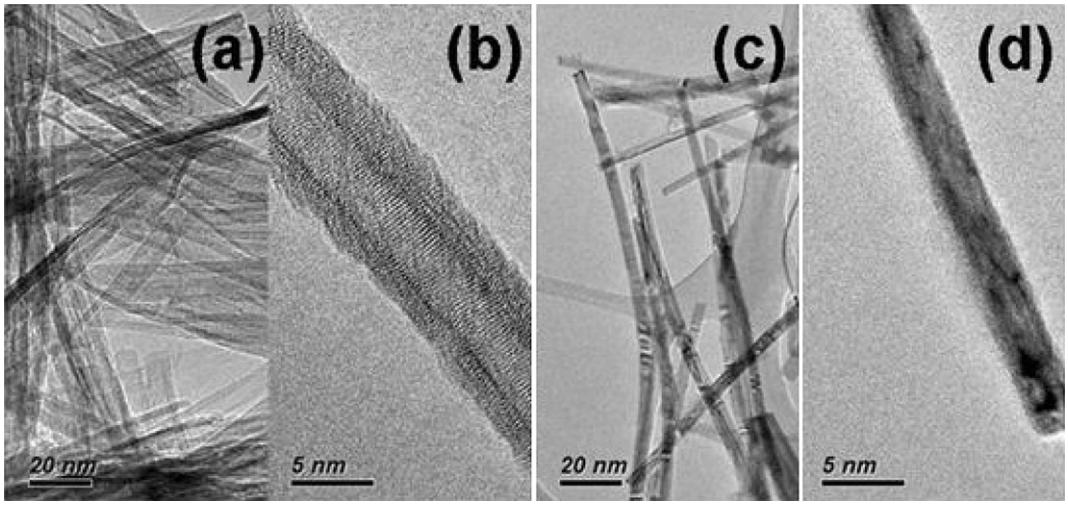

Fig. 1. (a-b) HRTEM image of MnO_2 nanotubes, and (c-d) MnO_2 nanowires.

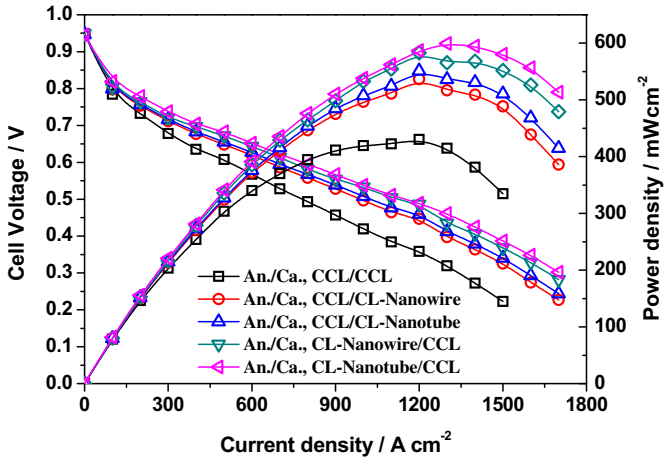

Fig. 3. Single cell performances of fuel cell with variable catalyst layer.

significantly from 0.943 to 0.687 V during the 5000 min. The OCV reduction rate was 51.2 μV min^{-1}. The OCV for the fuel cell assembled by catalyst layer with MnO_2 nanotubes and catalyst layer with MnO_2 nanowire as the cathodes and conventional catalyst layer as the anodes decreased from 0.943 to 0.749 V, and 0.942 to 0.745 V during the accelerating test, respectively. The OCV degradation rates were 38.8 μV s^{-1} and 39.4 μV s^{-1}. The OCV reduction rate of the catalyst layer with MnO_2 was much lower than that of the conventional catalyst layer demonstrated the radical scavenge of the MnO_2 in the catalyst layer. When MnO_2 is used as the anodes, the OCV reduction rates were further decreased because, in an operated fuel cell at OCV or low current density condition, hydrogen peroxide and radical are trends to be generated in the anode at low current density [20,35,36]. The OCV for the fuel cell assembled by catalyst layer with MnO_2 nanotubes and catalyst layer with MnO_2 nanowires as the anodes and conventional catalyst layer as the cathode decreased from 0.938 to 0.845 V,

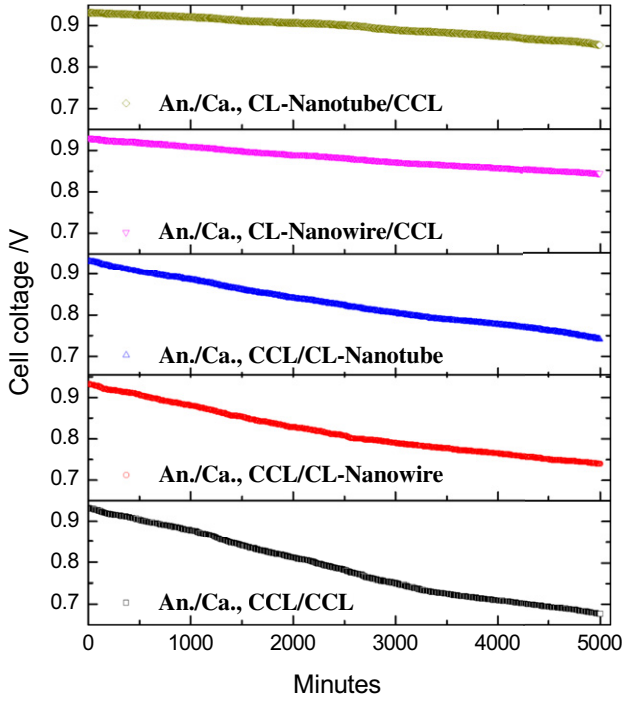

Fig. 4. Open circuit voltage (OCV) degradation of fuel cell with variable catalyst layer.

and 0.936 to 0.851 V during the accelerating test, respectively. The OCV degradation rates were 18.6 μV s^{-1} and 17.0 μV s^{-1}.

Fig. 5 depicts cyclic voltammograms for the various catalyst layers after 5000 min acceleration. The H_2 desorption peaks provide the information of the electrochemical active surface of Pt. The clear appearance of hydrogen peaks indicates that the 'triple-phase boundaries' where the electrolyte, reaction materials, and electrically connected catalyst particles still contact together in catalyst layer after the durability tests. The conventional catalyst layer as a cathode in the cell presents a large degradation from 180.2 cm^2 cm^{-2} to 83.6 cm^2 cm. Catalyst layer with MnO_2 nanotubes and catalyst layer with MnO_2 nanowire as cell anodes also have degradation after the acceleration. The electrochemical active surface areas degraded from 177.8 to 90.3 cm^2 cm^{-2}, and 178.3 to 95.2 cm^2 cm^{-2}, respectively. However, the catalyst layer with MnO_2 has less degradation if used as cathodes. The surface areas for catalyst layer with MnO_2 nanotubes and catalyst layer with MnO_2 nanowire as cathodes after acceleration are 99.5 cm^2 cm^{-2} and 104.6 cm^2 cm^{-2}, respectively. This result demonstrated for the same materials, the anodic degradation is much larger than the cathode because of more radicals are generated in anode at low current density. However, the open circuit voltage (OCV) degradation (Fig. 3) of cells assembled by catalyst layer with MnO_2 as cathode were much higher than the cells as anode, implies that electrolyte membrane degradation by the radical contributed much to the cell degradation.

Hydrogen permeation across the proton exchange membrane was measured by crossover current. Since hydrogen permeability is a function of the hydration and temperature of the membrane [37–39], measurements were taken at the controlled temperature and humidification conditions of 60 °C, 100% RH%. Fig. 6 shows linear sweep voltammograms of cells before and after the OCV accelerated degradation. Typical fresh cell have low hydrogen crossover with *ca.* 1.72 mA cm^{-2}. However, for a cell with conventional catalyst layer in both anode and cathode, the hydrogen crossover through the MEA increased to 14.7 mA cm^{-2}. Applying the MnO_2 in the cathode catalyst layer slightly reduced the membrane degradation. The hydrogen crossover of cell assembled by catalyst layer with MnO_2 nanowires in cathode and conventional catalyst layer in anode, catalyst layer with MnO_2 nanotubes in cathode and conventional catalyst layer in anode are about 11.4 and 9.5 mA cm^{-2}, respectively. However, applying the one-dimensional MnO_2 in the anode extensively minimize the radical corrosion of the electrolyte membrane because the radical generated mostly in

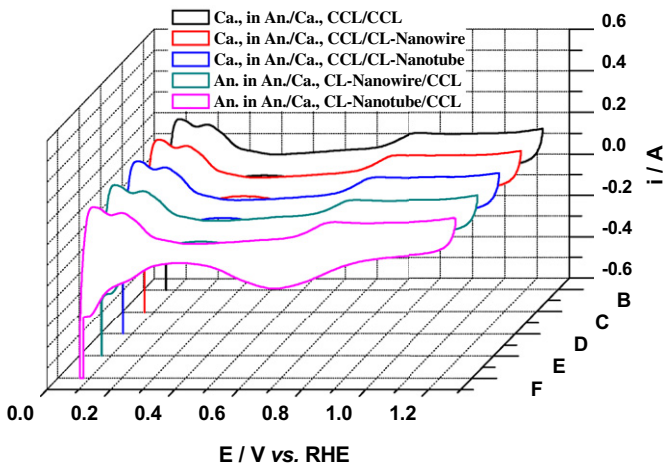

Fig. 5. Cyclic voltammograms of the variable catalyst layer in the single cells after OCV accelerated degradation.

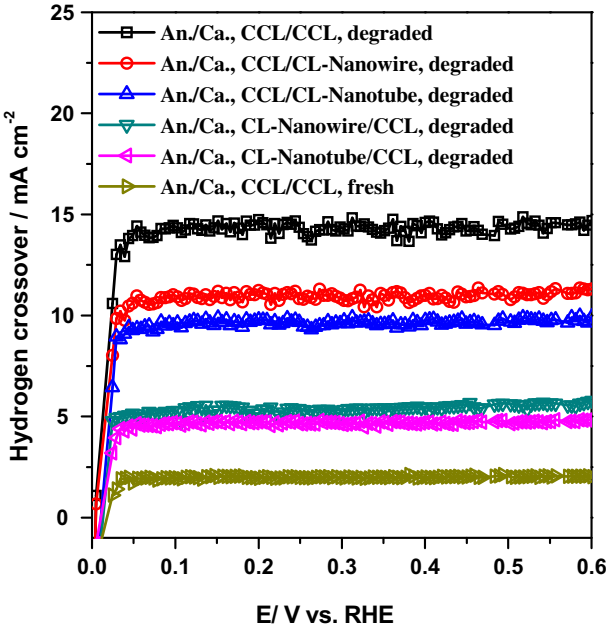

Fig. 6. Hydrogen permeation of the cells assembled with variable catalyst layer.

the anode. After the OCV degradation, the hydrogen crossover of cell assembled by catalyst layer with MnO_2 nanowires in anode and catalyst layer with MnO_2 nanotubes in cathode are about 5.3 and 4.9 mA cm^{-2}, respectively. Thus, radical scavenge MnO_2 in the anodic catalyst is an effective strategy that minimize the radical degradation in PEM fuel cells at OCV condition.

4. Conclusions

1D MnO_2 nanotubes and nanowires with sizes of 5–8 nm in diameter and more than 100 nm in length were successfully fabricated by facile hydrothermal methods. These 1D MnO_2 scavengers in the anodic catalyst layer is an effective strategy that minimizes the radical degradation in PEM fuel cells. Water retention of the hydrophilic 1D MnO_2 can reduce the humidity sensitivity of the fuel cells. At 75 RH% humidify levels of inlet gas at 60 °C, Single cells assembled by catalyst layer with MnO_2 nanotubes and with nanowires as the anodes have peak power densities of 599.3 mW cm^{-2} and 583.2 mW cm^{-2}, respectively, better than a single cell assembled by conventional catalyst layer in cathode and anode (430.4 mW cm^{-2}). After the OCV degradation, the hydrogen crossover of cell assembled by catalyst layer with MnO_2 nanowires or MnO_2 nanotubes in anode and traditional catalyst layer cathode are about 5.3 and 4.9 mA cm^{-2}, respectively. As a comparison, single cell with conventional catalyst layer in both anode and cathode, the hydrogen crossover through the MEA is increased to 14.7 mA cm^{-2}.

Acknowledgements

This work was financially supported by The National Basic Research Program of China (Grant No. 2013CB932901, 2010CB923200) and National Natural Science Foundation of China (Grant No. 51102019, 61177085, 60937003, 51172030, 51172208, 51272031).

References

[1] R. Lin, B. Li, Y.P. Hou, J.M. Ma, Int. J. Hydrog. Energy 34 (2009) 2369.
[2] X.Z. Yuan, S. Zhang, H. Wang, J. Wu, J.C. Sun, R. Hiesgen, K.A. Friedrich, M. Schulze, A. Haug, J. Power Sources 195 (2010) 7594.
[3] H.L. Tang, P.K. Shen, S.P. Jiang, W. Fang, P. Mu, J. Power Sources 170 (2007) 85.
[4] H. Zhang, P.K. Shen, Chem. Rev. 112 (2012) 2780.
[5] F. Wang, H.L. Tang, M. Pan, D.X. Li, Int. J. Hydrog. Energy 33 (2008) 2283.
[6] H.L. Tang, M. Pan, F. Wang, P.K. Shen, S.P. Jiang, J. Phys. Chem. B 111 (2007) 8684.
[7] S.J. Ashton, M. Arenz, Electrochem. Commun. 13 (2011) 1473.
[8] J. Chen, J.B. Siegel, T. Matsuura, A.G. Stefanopoulou, J. Electrochem. Soc. 158 (2011) B1164.
[9] C.C. Hung, P.Y. Lim, J.R. Chen, H.C. Shih, J. Power Sources 196 (2011) 140.
[10] A.A. Kulikovsky, J. Electrochem. Soc. 158 (2011) B957.
[11] M. Lei, P.G. Li, L.H. Li, W.H. Tang, J. Power Sources 196 (2011) 3548.
[12] M. Lei, S.L. Wang, L.H. Li, W.H. Tang, J. Power Sources 196 (2011) 1123.
[13] S.S. Zhang, X.Z. Yuan, H.J. Wang, W. Merida, H. Zhu, J. Shen, S.H. Wu, J.J. Zhang, Int. J. Hydrog. Energy 34 (2009) 388.
[14] A.A. Shah, T.R. Ralph, F.C. Walsh, J. Electrochem. Soc. 156 (2009) B465.
[15] C. Zhou, M.A. Guerra, Z.M. Qiu, T.A. Zawodzinski, D.A. Schiraldi, Macromolecules 40 (2007) 8695.
[16] X. Fang, P.K. Shen, S.Q. Song, V. Stergiopoulos, P. Tsiakaras, Polymer Degrad. Stab. 94 (2009) 1707.
[17] Y. Cheng, H. Tang, M. Pan, J. Power Sources 198 (2012) 190.
[18] H. Hori, M. Murayama, T. Sano, S. Kutsuna, Ind. Eng. Chem. Res. 49 (2010) 464.
[19] A. Pozio, R.F. Silva, M. De Francesco, L. Giorgi, Electrochim. Acta 48 (2003) 1543.
[20] J.M. Noel, A. Latus, C. Lagrost, E. Volanschi, P. Hapiot, J. Am. Chem. Soc. 134 (2012) 2835.
[21] Y. Nosaka, K. Ohtaka, N. Ohguri, A.Y. Nosaka, J. Electrochem. Soc. 158 (2011) B430.
[22] L. Gubler, S.M. Dockheer, W.H. Koppenol, J. Electrochem. Soc. 158 (2011) B755.
[23] N. Ohguri, A.Y. Nosaka, Y. Nosaka, J. Power Sources 195 (2010) 4647.
[24] M. Arenz, V. Stamenkovic, T.J. Schmidt, K. Wandelt, P.N. Ross, N.M. Markovic, Surf. Sci. 523 (2003) 199.
[25] P. Trogadas, J. Parrondo, V. Ramani, Chem. Commun. 47 (2011) 11549.
[26] P. Trogadas, J. Parrondo, F. Mijangos, V. Ramani, J. Mater. Chem. 21 (2011) 19381.
[27] P. Trogadas, J. Parrondo, V. Ramani, Electrochem. Solid State Lett. 11 (2008) B113.
[28] P. Trogadas, V. Ramani, J. Power Sources 174 (2007) 159.
[29] J. Howsawkeng, A.L. Teel, T.F. Hess, R.L. Crawford, R.J. Watts, Sci. Total Environ. 409 (2010) 439.
[30] D. Zhao, B.L. Yi, H.M. Zhang, H.M. Yu, J. Membr. Sci. 346 (2010) 143.
[31] L. Zhang, Y. Nie, C. Hu, X. Hu, J. Hazard. Mater. 190 (2011) 780.
[32] H.L. Tang, S.L. Wang, S.P. Jiang, M. Pan, J. Power Sources 170 (2007) 140.
[33] A. Ohma, S. Yamamoto, K. Shinohara, J. Power Sources 182 (2008) 39.
[34] W. Yoon, X.Y. Huang, J. Electrochem. Soc. 157 (2010) B599.
[35] A. Kishi, S. Shironita, M. Umeda, J. Power Sources 197 (2012) 88.
[36] A. Kishi, M. Inoue, M. Umeda, J. Phys. Chem. C 114 (2010) 1110.
[37] C. Francia, V.S. Ijeri, S. Specchia, P. Spinelli, J. Power Sources 196 (2011) 1833.
[38] Y. Shibahara, H.S. Sodaye, Y. Akiyama, S. Nishijima, Y. Honda, G. Isoyama, S. Tagawa, J. Power Sources 195 (2010) 5934.
[39] M. Inaba, T. Kinumoto, M. Kiriake, R. Umebayashi, A. Tasaka, Z. Ogumi, Electrochim. Acta 51 (2006) 5746.